The effects of predominant nonlinear hydrodynamics on the power absorption performance of a heaving point absorber adopting linear control principles

Ocean Engineering 325 (2025) 120774

Contents lists available at ScienceDirect

Ocean Engineering

journal homepage: www.elsevier.com/locate/oceaneng

Research paper

The effects of predominant nonlinear hydrodynamics on the power absorption performance of a heaving point absorber adopting linear control principles

Yifeng Gu [a,*], Boyin Ding [a], Nataliia Y. Sergiienko [a], Benjamin S. Cazzolato [a], Giuseppe Giorgi [b]

[a] School of Electrical and Mechanical Engineering, The University of Adelaide, Adelaide, South Australia, 5000, Australia
[b] Marine Offshore Renewable Energy (MOREnergy) Lab, Department of Mechanical and Aerospace Engineering (DIMEAS), Politecnico di Torino, Turin, 5000, Italy

ARTICLE INFO

Keywords:
Point absorber
Nonlinearities
Power take-off control
Froude–Krylov force

ABSTRACT

The power performance capability of a point absorber (PA) wave energy converter (WEC) is highly dependent on the design of the power take-off (PTO) controller, which plays a significant role in maximising power absorption efficiency. The wave-body interaction hydrodynamics are usually assumed to have a linear behaviour in the design optimisation of point absorbers, including PTO controllers. However, unavoidable nonlinearities in reality may violate the commonly used linear assumptions in the design of optimal WEC PTO controllers. This paper aims to introduce/include predominant nonlinear hydrodynamics, including the nonlinear Froude–Krylov (NLFK) forces experienced by a semi-submerged spherical heaving PA (HPA). The impacts of these nonlinear forces on the power absorption of the most commonly used linear controller is investigated in regular waves to validate the efficacy of applying linear control principles in a close-to-real environment. The main findings of this study are: for a semi-submerged PA under medium to high sea states in regular waves (i) the linear power maximising control principles underestimate the absorbed power by up to 54 % under NLFK forces; (ii) both dynamic NLFK and viscous drag forces have significant impacts (up to 57 %) on the power absorption efficiency of WEC systems; and (iii) tuning of traditional linear spring-damper control can achieve maximum power absorption under predominant nonlinear hydrodynamics, similar to that under multi-resonant control.

1. Introduction

Due to the world's growing demand for renewable power, ocean wave energy has been attracting researchers' interest over the past 200 years due to its persistence, high energy density and predictability (Falnes and Perlin, 2003). A wave energy converter (WEC) is a device that converts ocean wave energy into useful electricity. In general, WECs may be classified as including a terminator, an attenuator, a point absorber (PA), or a quasi-point absorber on the basis of their relative dimensions and orientation to the propagating wave (Sergiienko, 2018). According to the data provided in Agency (2014), PAs account for 53 % of the existing prototypes, and are one of the simplest and most promising concepts attracting intensive research interest among WEC technologies (Kara, 2020). Although wave energy may have superior characteristics over other types of renewable energy (e.g., wind, solar, etc.), it is not competitive in the energy market because the development of WEC technologies is still at an immature stage (Guo and Ringwood, 2021). One of the major reasons is the lack of the power take-off (PTO) controller with intuitive structure, which can achieve high power conversion efficiency while retaining low costs under the real-time industrial applications. The existence of various types of nonlinearities in reality is one of the main obstructions complicating the PTO controller design requirements (Penalba et al., 2017).

Linear wave theory is the fundamental principle for the WEC modelling and controller designs of WEC systems under small motions. It assumes the water depth is uniform and the fluid flow is inviscid, irrotational and incompressible (Falnes, 2002). In reality, WECs are designed to maximise power absorption by oscillating the device with large buoy motions, in particular under medium to high sea states. Consequently, the hypotheses under which linear wave theory is valid becomes restrictive, especially the assumption of small motions (Giorgi and Ringwood, 2017b). WEC systems will exhibit nonlinear behaviours given different sources, such as interactions between the WEC body and fluid, and nonlinear dynamics in the PTO machinery (Bacelli and Coe, 2020; Penalba et al., 2017). To fully consider the implication of nonlinearities on the performance of PTO controllers, they need to be simulated properly in WEC systems.

* Corresponding author.
E-mail address: yifeng.gu@adelaide.edu.au (Y. Gu).

https://doi.org/10.1016/j.oceaneng.2025.120774
Received 8 September 2024; Received in revised form 8 February 2025; Accepted 21 February 2025
Available online 4 March 2025

Most previous studies ignored or linearised the nonlinearities in a linear-wave-theory-based model (LM), and thus WEC systems were forced to show a linear behaviour due to the need for simplicity and computational convenience for simulations (Do, 2022). It is convenient to analyse the impact of each linearised hydrodynamic force on the performance of PTO controllers in LM. However, there are significant discrepancies between the hydrodynamic behaviour of LM and experimental tank tests under medium to high sea states (Babarit et al., 2009). The power efficiency of PTO is consequently overestimated in these sea states. Some studies implemented a fully nonlinear Computational Fluid Dynamics (CFD) approach to simulate and analyse the survivability of WECs. CFD solver can simulate various nonlinear hydrodynamics simultaneously in high-fidelity models, so the complex hydrodynamic behaviours are observed through a vast amount of information about WECs provided after each simulation. Consequently, the computational burden of the CFD approach is very high, and the numerical nature of the method is not as useful as linear wave theory in analytical studies of power maximising controls. Thus, there are very few studies applying CFD to PTO control (Davidson and Costello, 2020). As a compromise between computational efforts and model fidelity, partially nonlinear models are therefore proposed for WEC controller design purposes. For example, NLFK4ALL is an open-source demonstration toolbox that only considers the predominant nonlinear Froude–Krylov (NLFK) force for PAs in a computationally efficient way (Giorgi , 2019), while the other hydrodynamic forces remain linear.

On the other hand, there is a wide range of control strategies tested and implemented in WEC applications (Guo and Ringwood, 2021). There are few nonlinear controllers (e.g., nonlinear model predictive control) designed to improve the power performance of WECs, considering the impact of nonlinear hydrodynamics under medium to high sea states (Richter et al., 2012; Faedo et al., 2022b). However, these controllers usually face challenges associated with real-time implementation and robustness (Falnes, 1995; Tedd and Frigaard, 2007). Most of the controllers are still derived from linear wave theory, following linear control principles (e.g., well known approximate velocity tracking (AVT), or approximate complex conjugate control (ACC)) in small sea waves (Bacelli and Coe, 2020). These controllers are capable of maximising energy absorption from incoming waves with mild computational requirements, often intuitive in their design; hence, especially appealing for real-time industrial applications (Faedo et al., 2022a). However, their performance, subject to nonlinear hydrodynamics under medium to high sea states, remains questionable.

The motivation of this paper is to answer the following research questions regarding the ongoing controversies between nonlinear hydrodynamics (reality) and linear PTO control (feasibility in implementation), based on a semi-submerged PA: (i) What are the limitations of linear control principles on the power performance of a semi-submerged spherical HPA exhibiting nonlinear dynamics? (ii) Is it possible or necessary to improve the linear control principles to maximise the absorbed power under predominant nonlinear dynamics? The novelty of this paper is to: (i) tackle the evaluation of different control strategies with predominant nonlinearities in a systematic way, using the computationally efficient NLFK method, not yet widely used in the literature for optimal control; and (ii) propose and evaluate the potential benefits of multi-resonant control with a nonlinear model.

The methodology framework is designed to explore the research questions, with the details presented in Section 2.1. The WEC system is described in Section 2.2, including WEC modellings and controller designs. The results to demonstrate the research questions will be discussed in Section 3.

2. Methodology

In this section, the framework will be stated first to reveal the reasons of selecting the predominant hydrodynamic nonlinearities, and linear controllers. The characteristics of the HPA will be stated in Section 2.2.

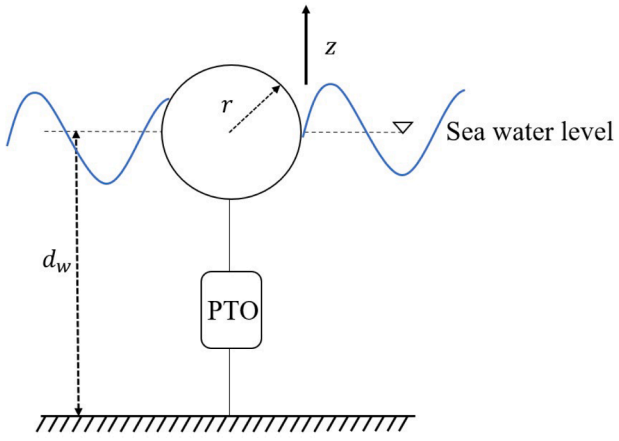

Fig. 1. A semi-submerged spherical heaving point absorber.

The definition of various hydrodynamic forces will be introduced in Section 2.3. Both linear and partially nonlinear models and the setting of controllers will be proposed separately, and the simulation setup will be clarified.

2.1. Methodology framework

To simulate appropriate partially nonlinear models, the predominant nonlinear hydrodynamic forces need to be identified first. If the body of a WEC is much smaller than the wavelength for a semi-submerged buoy (e.g., PAs), viscous drag and NLFK forces become relevant to the performance of WEC systems once the wave height increases to medium to high sea states, while the impacts of nonlinear diffraction and radiation are minor (Falnes, 2002; Merigaud et al., 2012; Gilloteaux et al., 2008; Giorgi and Ringwood, 2018). Further studies stated that the performance of a spherical PA is more easily impacted by NLFK force than other shapes of buoys (Kim et al., 2021; Penalba Retes et al., 2015). Regarding the modes of WECs, the dominance of NLFK in heave is more significant than that in surge/pitch (Folley, 2016).

On the other hand, complex conjugate control (CCC), also known as impedance matching control, is one of the most well-known linear controllers to achieve the maximum power absorption in regular waves (Falnes and Perlin, 2003; Gu et al., 2021). ACC is a simple and reliable control strategy derived from CCC taking real-time implementation into consideration (Bacelli and Coe, 2020; Gu et al., 2021). Spring-damper is the simplest form of ACC following linear wave theory. It is sometimes called proportional-integral (PI), using WEC velocity as a basis. Another way to approximate CCC has been proposed in Song et al. (2016); Abdelkhalik et al. (2017); Coe et al. (2017). It is called multi-resonant control, where multiple parallel PI controllers act simultaneously targeting individual signals at each wave frequency in the wave spectrum. Multi-resonant control is a wide band controller that can decompose the WEC control problems (e.g., tuning and stability) into sub-problems. However, the previous studies only tested the performance of multi-resonant control in a linear model, so the impact of nonlinear hydrodynamics on that still needs more investigation.

2.2. System description of WEC

A spherical semi-submerged HPA is selected in this study, to consider the most extreme impact of nonlinearities (e.g., NLFK force) on WEC systems compared with other shapes and modes of PAs, which is shown in Fig. 1. The buoy is assumed to have pure heaving motion only. Table 1 shows corresponding system parameters, where m is the mass of the buoy; r is the radius of the buoy; d_w is the water depth, ρ is the density of water; and g is the gravitational acceleration.

Table 1
Parameters of a spherical buoy.

Items	Value/unit
Buoy mass (m)	2.698×10^5 kg
Buoy radius (r)	5 m
Water depth (d_w)	infinite
Water density (ρ)	1024 kg/m^3
Gravitational acceleration (g)	9.8067 m/s^2

2.3. Hydrodynamic forces

Linear wave theory is commonly used to estimate the hydrodynamic forces acting on a structure, and Newton's second law can be applied to describe the WEC system dynamics in heave (Merigaud et al., 2012):

$$m\ddot{z}(t) = F_g - \iint_{S(t)} p(t)\vec{n}\, dS + F_{pto}(t), \tag{1}$$

where m is the mass of the buoy; z is the buoy displacement in heave relative to the still water level; F_g is the gravity force. $S(t)$ is the wetted surface of a buoy; $\vec{n}$ is the vector normal to the surface; p is the pressure acting on this surface, and F_{pto} is the PTO (control) force acting at the buoy's centre of gravity.

According to Bernoulli's equation, the pressure $p(t)$ can be obtained as follows (Newman, 2018):

$$p(t) = -\rho g z(t) - \rho\frac{\partial\phi(t)}{\partial t} - \rho\frac{|\nabla\phi(t)|^2}{2}, \tag{2}$$

where $\phi(t)$ is the potential flow of the wave describing the velocity field as the gradient of the velocity potential. Based on linear wave theory, $\phi(t)$ can be decomposed as:

$$\phi(t) = \phi_I(t) + \phi_D(t) + \phi_R(t), \tag{3}$$

where $\phi_I(t)$, $\phi_D(t)$ and $\phi_R(t)$ represent the undisturbed incident flow, the diffraction flow and the radiation flow separately. Substituting Eq. (3) into Eq. (2), the pressure for each potential can be defined as p_I, p_D and p_R respectively.

Combining Eqs. (1)–(3), different forces can be identified (Giorgi and Ringwood, 2017b):

- The Froude–Krylov force is split into two parts: static and dynamic forces, denoted as $F_{FK_{st}}$ and $F_{FK_{dy}}$ separately. The static force is formed by the gravity force and, the integral over the wetted surface of the static pressure $p_{st} = -\rho g z$:

$$F_{FK_{st}}(t) = F_g - \iint_{S(t)} p_{st}(t)\vec{n}\, dS. \tag{4}$$

  The dynamic force refers to the integral over the wetted surface of the dynamic pressure $p_{dy} = -\rho\frac{\partial\phi_I}{\partial t} - \rho\frac{|\nabla\phi_I|^2}{2}$:

$$F_{FK_{dy}}(t) = -\iint_{S(t)} p_{dy}(t)\vec{n}\, dS. \tag{5}$$

- As mentioned in Section 2.1, nonlinear computations of diffraction and radiation forces do not make a significant difference compared with that of linear forces for an HPA. Therefore, their computation is based on the mean wetted surface $S(0)$. The diffraction force (F_d) is shown as:

$$F_d(t) = -\iint_{S(0)} p_D(t)\vec{n}\, dS, \tag{6}$$

  where $p_d = -\rho\frac{\partial\phi_D}{\partial t} - \rho\frac{|\nabla\phi_D|^2}{2}$.
- Radiation force (F_r) is shown as:

$$F_r(t) = -\iint_{S(0)} p_R(t)\vec{n}\, dS, \tag{7}$$

  where $p_r = -\rho\frac{\partial\phi_R}{\partial t} - \rho\frac{|\nabla\phi_R|^2}{2}$.

Combining Eqs. (1) to (7), the WEC system dynamics can be rewritten as:

$$m\ddot{z}(t) = F_{FK_{st}}(t) + F_{FK_{dy}}(t) + F_d(t) + F_r(t) + F_{pto}(t). \tag{8}$$

2.4. Hydrodynamic models

LM is widely used in WEC studies, and one of the main reasons is that LM has sufficient accuracy and computational convenience to estimate the average power output of PTO system in small sea states (Sergiienko, 2018). Once the height of incoming wave increases, unavoidable nonlinearities may violate the linear wave theory, and thus the LM can be an inaccurate representation of an actual physical WEC system. Different from the CFD solver, the predominant nonlinear hydrodynamics can be introduced into LM separately to investigate the individual impact of these forces on the performance of PTO controllers. In this section, the mathematical expressions of linear and partially nonlinear models will be stated respectively.

2.4.1. Linear-wave-theory-based model (LM)

Based on linear wave theory, the free surface (η) is assumed at the still wave level $z = 0$, and the computations of hydrodynamic forces are based on the mean wetted surface, so the horizontal cross section area will not change with the incoming waves regardless of the shape of the buoy. Eq. (8) is rewritten as:

$$\underbrace{m\ddot{z}(t) + A_\infty\ddot{z}(t) + \int_{-\infty}^{t} B(t-\tau)\dot{z}(\tau)\, d\tau}_{F_r} + \underbrace{k_{hs}z(t)}_{F_{FK_{st}}} = \underbrace{F_{exc}(t)}_{F_{FK_{dy}}+F_d} + F_{pto}(t), \tag{9}$$

where A_∞ is the infinite-frequency added mass coefficient and $B(t)$ is the radiation impulse response function, depending on the motion history of the buoy. Both represent the radiation force. For simulations on the linear radiation effects in the time-domain, the convolution integral in Eq. (9) is normally replaced by a state-space model according to the methodology presented in Perez and Fossen (2009). As aforementioned, the computations of FK forces are based on the fixed mean wetted surface in a linear model, thus static FK force is linearised as the hydrostatic stiffness term, where $k_{hs} = \rho g S(0)$. For a spherical buoy, $S(0)$ is equal to πr^2. The linearised dynamic FK force is usually combined with the diffraction force as the linear excitation force F_{exc}, which is the force produced by the incident waves on the buoy. The linear hydrodynamic parameters including the excitation force, the frequency-dependent added mass and radiation damping in Eq. (9) are calculated by boundary-element potential methods (BEM). In general, BEM-based codes are commercial and open-source, such as NEMOH used in this study (Babarit and Delhommeau, 2015).

2.4.2. Partially nonlinear models

To simulate a more close-to-real environment than LM, the predominant static and dynamic NLFK, and viscous drag forces need to be introduced into the LM separately.

LM with nonlinear dynamic Froude–Krylov force. Substituting Eq. (5) into (9), the WEC system dynamics can be rewritten as:

$$\underbrace{m\ddot{z}(t) + A_\infty\ddot{z}(t) + \int_{-\infty}^{t} B(t-\tau)\dot{z}(\tau)\, d\tau}_{F_r} + \underbrace{k_{hs}z(t)}_{F_{FK_{st}}} = -\iint_{S(t)} p_{dy}(t)\vec{n}\, dS + F_d(t) + F_{pto}(t), \tag{10}$$

where the dynamic FK force is the only nonlinear term. The other hydrodynamic forces, such as radiation force, static FK force, and diffraction force, are kept linear. In the computation of NLFK force, the free surface elevation (η) changes with time $z = \eta^I(x, y, t)$, and NLFK force needs to be computed over the instantaneous wetted surface at each time step $S(t)$. Therefore, the performance of NLFK force is closely related to the free surface elevation and the buoy motion.

LM with nonlinear static Froude–Krylov force. Substituting Eq. (4) into Eq. (9), the WEC system dynamics can be rewritten as:

$$m\ddot{z}(t) + \underbrace{A_\infty \ddot{z}(t) + \int_{-\infty}^{t} B(t-\tau)\dot{z}(\tau)\, d\tau}_{F_r} + \iint_{S(t)} p_{st}(t)\vec{n}\, dS = \underbrace{F_{exc}(t)}_{F_{FK_{dy}}+F_d} + F_{pto}(t) + F_g, \tag{11}$$

where only the static FK force is nonlinear, while the other hydrodynamic forces, such as radiation force, dynamic FK force, and diffraction force, are kept linear.

LM with viscous drag force. Viscous drag force is one of the most common nonlinear hydrodynamic forces implemented in WEC fields. Although some investigation stated that the magnitude of the viscous drag force is minor compared with other hydrodynamic forces for an HPA with a large body in selected sea states (Giorgi and Ringwood, 2018), the impact of viscous drag on the performance of linear control principles still needs more investigation. The calculation of viscous drag follows the Morison equation (Morison et al., 1950):

$$F_{vd}(t) = -\frac{1}{2}\rho C_D A_D |\dot{z} - \dot{z}_0|(\dot{z} - \dot{z}_0), \tag{12}$$

where C_D is the drag coefficient. For a spherical buoy, C_D is estimated to be 0.5 based on empirical choice for simplification (Giorgi and Ringwood, 2017a). A_D is the horizontal cross-sectional area of a buoy perpendicular to the incident wave; $\dot{z}_0$ is the fluid velocity at the center of mass of the buoy undisturbed, which is assumed to be negligible compared to the buoy velocity in this paper (Al Shami et al., 2021; Gobato et al., 2016). Introducing Eq. (12) into Eq. (9), the WEC system dynamics can be rewritten as:

$$m\ddot{z}(t) + \underbrace{A_\infty \ddot{z}(t) + \int_{-\infty}^{t} B(t-\tau)\dot{z}(\tau)\, d\tau}_{F_r} + \underbrace{k_{hs} z(t)}_{F_{FK_{st}}} + \frac{1}{2}\rho C_D A_D |\dot{z}(t)|\dot{z}(t) = \underbrace{F_{exc}(t)}_{F_{FK_{dy}}+F_d} + F_{pto}(t), \tag{13}$$

where only the viscous drag force is nonlinear, while the other predominant hydrodynamic forces (e.g., both static and dynamic FK forces) are kept linear. In many existing studies (Sergiienko et al., 2017), the nonlinear viscous term $F_{vd}(t)$ can be linearised as a damping coefficient (B_{vd}^{ω}) through Lorentz Linearisation (Terra et al., 2005), which changes with wave heights and frequencies. The linearised damping force can account for nonlinear F_{vd} whilst maintaining the same amount of energy dissipated.

LM with predominant hydrodynamic nonlinearities. Taking predominant hydrodynamic nonlinearities (e.g., static and dynamic NLFK, viscous drag) into consideration, the WEC model can be rewritten as:

$$m\ddot{z}(t) + \underbrace{A_\infty \ddot{z}(t) + \int_{-\infty}^{t} B(t-\tau)\dot{z}(\tau)\, d\tau}_{F_r} + \frac{1}{2}\rho C_D A_D |\dot{z}(t)|\dot{z}(t) + \iint_{S(t)} p_{st}(t)\vec{n}\, dS = \iint_{S(t)} p_{dy}(t)\vec{n}\, dS + F_d(t) + F_{pto}(t) + F_g. \tag{14}$$

2.5. Linear power take-off controller settings

Following the principle of CCC control, the mathematical derivation of optimal conditions for maximising the absorbed power of WEC will be stated in Section 2.5.1. Based on that, two typical linear ACC controls (PI and multi-resonant controls) will be shown in Sections 2.5.2 and 2.5.3 separately.

2.5.1. Linear optimal power maximising principles of complex-conjugate control

In general, a linear force-to-velocity model of a PA WEC in the frequency domain can be used to describe the WEC system:

$$\frac{u(\omega)}{F_{exc}(\omega)} = \frac{1}{Z_i(\omega) + Z_{pto}(\omega)}, \tag{15}$$

where $u(\omega)$ is the buoy's complex amplitude of velocity; $Z_i(\omega)$ is the frequency-dependent system intrinsic impedance (associated with wave-structure interaction dynamics) as described in Eq. (8); $Z_{pto}(\omega)$, the frequency-dependent optimal PTO load impedance (associated with the PTO control force), is introduced to modify the overall system behaviour. Therefore, when a PI control is selected as a controller, these two impedances are given by (Ringwood et al., 2014):

$$Z_i(\omega) = B^{\omega} + j\omega\left(m + A^{\omega} - \frac{k_{hs}}{\omega^2}\right), \tag{16}$$

$$Z_{pto}(\omega) = \underbrace{B_{pto}}_{\text{Proportional}} \underbrace{-j\frac{K_{pto}}{\omega}}_{\text{Integral}}, \tag{17}$$

where $B^{\omega} = B_r^{\omega} + B_{vd}^{\omega}$ is a part of the wave dynamics, and B_r^{ω} and A^{ω} are the wave frequency-dependent radiation damping coefficient and added mass of the buoy obtained from NEMOH. When the viscous drag is not considered in the WEC system, $B_{vd}^{\omega} = 0$; B_{pto} and K_{pto} are the damping and stiffness coefficient in the PTO control, respectively, assuming that the PTO control is a combination of an integral/spring control and proportional/linear damper control; CCC defines the following complex conjugate relationship between system intrinsic impedance and the PTO load impedance for maximising the power absorption of a point absorber WEC:

$$Z_{pto}(\omega) = Z_i^*(\omega), \tag{18}$$

where $()^*$ denotes the complex conjugate.

Optimal resonance condition. Substituting Eqs. (16) and (17) into (18), the first optimal power absorption condition can be obtained:

$$K_{pto} = \omega^2(m + A^{\omega}) - k_{hs}. \tag{19}$$

Eq. (19) shows the WEC resonance condition. When the natural frequency of the system is equal to the frequency of the excitation force, the system will be in resonance, so the maximum wave power can be absorbed into the WEC system. At the resonant frequency, the total restoring (spring) forces, including the hydrostatic spring force and the mass-acceleration force, are anti-phase and thus cancel each other out.

Optimal amplitude condition. The optimal amplitude condition is shown as:

$$B_{pto} = B_r^{\omega} + B_{vd}^{\omega}. \tag{20}$$

When the viscous drag is ignored in the WEC system, $B_{vd}^{\omega} = 0$, and $B_{pto} = B_r^{\omega}$. When the PTO damping in the controller is above the optimal value, the motion amplitude will be too small, which will decrease the power absorption. Otherwise, the motion amplitude will be too large so power is radiated back to the sea.

Based on the optimal resonance and amplitude conditions, the optimal buoy velocity is obtained:

$$u_{opt}(\omega) = \frac{F_{exc}(\omega)}{B^{\omega} + B_{pto}}, \tag{21}$$

where $u(\omega)$ is the buoy amplitude of velocity; Eq. (21) also demonstrates that the buoy velocity is in phase with the excitation force under optimal conditions (the phase difference of their time series becomes zero) and the overall system impedance becomes larger.

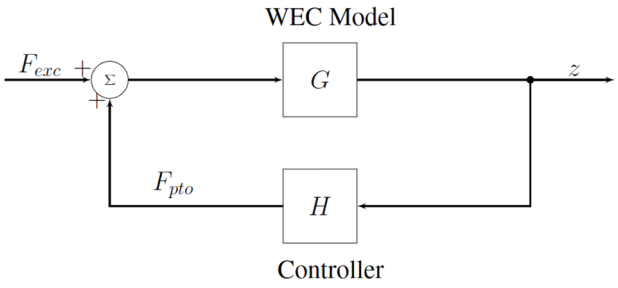

Fig. 2. Block diagram of a WEC system with PI control.

2.5.2. Proportional-integral (PI) control

The most well-known and commonly used ACC control for maximising WEC power absorption is a spring-damper control law (or more generally termed the PI controller in control discipline, using WEC velocity as a basis). In time domain, it is stated as:

$$F_{pto}(t) = \underbrace{-B_{pto}\dot{z}(t)}_{\text{Proportional}} \underbrace{-K_{pto}z(t)}_{\text{Integral}}. \tag{22}$$

When the nonlinearities are not considered in WEC systems, the optimal K_{pto} and B_{pto} can be obtained following Eqs. (19) and (20). Otherwise, the optimal control gains have to be found via a grid search (Gu et al., 2021), which is a simplex algorithm to set variations on both K_{pto} and B_{pto} to find out the maximum absorbed power. Fig. 2 shows the block diagram of the WEC system with PI control, where the Laplace domain annotation (s) is omitted for brevity. Substituting Eqs. (19) and (20) into (16) and (17),the WEC dynamics is denoted as $G(s)$ in Laplace domain derived from Eq. (16):

$$G(s) = \frac{s}{(m + A^{\omega})s^2 + (B_r^{\omega} + B_{vd}^{\omega})s + k_{hs}}. \tag{23}$$

The PI controller dynamics is denoted as $H(s)$ in Laplace domain derived from Eq. (17):

$$H(s) = \frac{-(B_r^{\omega} + B_{vd}^{\omega})s - \omega^2(m + A^{\omega}) + k_{hs}}{s}. \tag{24}$$

2.5.3. Multi-resonant control

Multi-resonant control was initially proposed to improve the power performance of WEC systems in irregular waves in LM (Song et al., 2016; Coe et al., 2017). The ocean wave free surface elevation is usually represented by the wave spectrum in irregular waves, which includes signals with different wave frequencies, amplitudes, phases and directions (MARINTEK and Norway, 2002). Multi-resonant control can implement a real-time decomposition of the measurement signal (e.g., the excitation force or buoy displacement) into multiple frequency components. Then, a separate optimal PI controller can be set at each frequency in the spectrum, as shown in Fig. 3, and this generates energy similar to complex conjugate control (Song et al., 2016). In Fig. 3, N is the number of wave frequencies, and excitation force (F_{exc}) is decomposed into different components (F_{exc1}, F_{exc2}, …, F_{excN}). In each separate component, $G(s)$ and $H(s)$ are WEC and PI control dynamics at each wave frequency. If nonlinearities are not considered, PI control can parallely achieve the optimisation of WEC systems following the linear optimal control principles in Eqs. (19) and (20), and the optimal velocity can be obtained analytically following Eq. (21).

Different from the previous studies of multi-resonant control in irregular waves in LM, in this study, due to the hydrodynamic nonlinearities (e.g., NLFK force), the measurement signal in the WEC system may be asymmetric in regular waves (Giorgi, 2024). The combination of dynamic NLFK and linear diffraction forces proposes a nonlinear excitation force, which is shown in Fig. 4, where the wave frequency is 0.89 rad/s (7 s wave period) and the wave height is 2 m as an example. Nonlinear

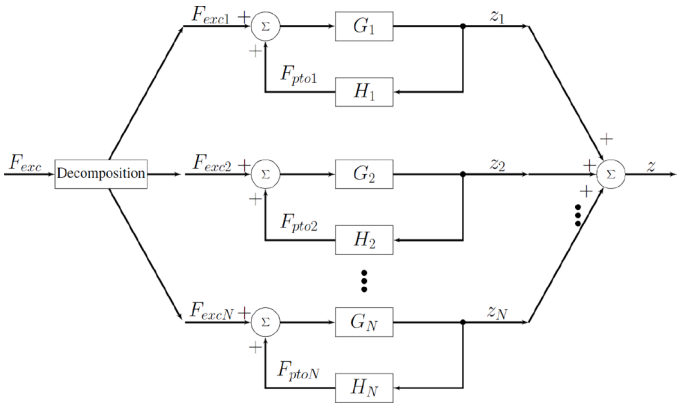

Fig. 3. Block diagram of a WEC system with multi-resonant control.

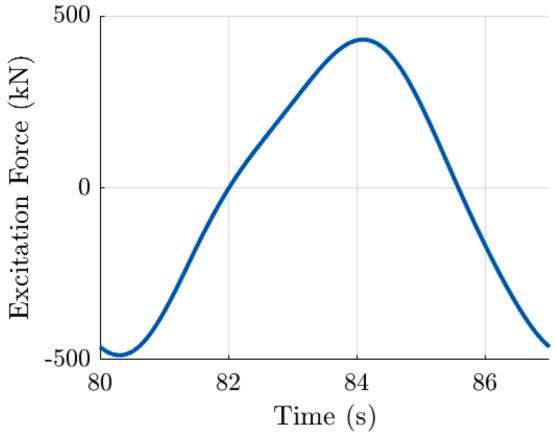

Fig. 4. Time series example of nonlinear excitation force.

signals can cause power reduction and instability problems for PTO controllers. To further analyse this behaviour, Fast Fourier Transforms (FFT) was proposed to decompose the signal into different harmonics (Song et al., 2016). As shown in Fig. 5a, except the signal at the fundamental frequency (0.89 rad/s), there are other two harmonics at 1.80 rad/s and 2.69 rad/s respectively, whose frequencies are twice and three times of the fundamental one. FFT is able to decompose the nonlinear F_{exc} into three separate signals with different amplitudes and phases (shown in Fig. 5b–d separately). Note that these decomposed signals are symmetrical and have linear behaviour, so they can be controlled by linear controllers. On the other hand, to achieve signal decomposition, least squares methods and Kalman Filter were also proposed in Abdelkhalik et al. (2017); Abdelkhalik and Zou (2019), and it was demonstrated that the Kalman Filter can accelerate the signal processing calculations compared with other two methods. Therefore, the Kalman filter is tuned and implemented in this paper.

Under the hydrodynamic nonlinearities, conventional PI control mainly controls the WEC performance at the fundamental frequency, while the impact of signals from harmonics 2 and 3 on the power performance of WEC systems still needs more investigation. For a complex time-series signal including multiple harmonics, multi-resonant control can decompose the control problem (e.g., tuning, stability) into subproblems, which is verified in the linear model in Song et al. (2016). However, the performance of multi-resonant control under hydrodynamic nonlinearities is still lacking in the literature.

2.6. Simulation setup

Regarding the NLFK modelling in the time domain, there is a computationally efficient demonstration toolbox called NLFK4ALL

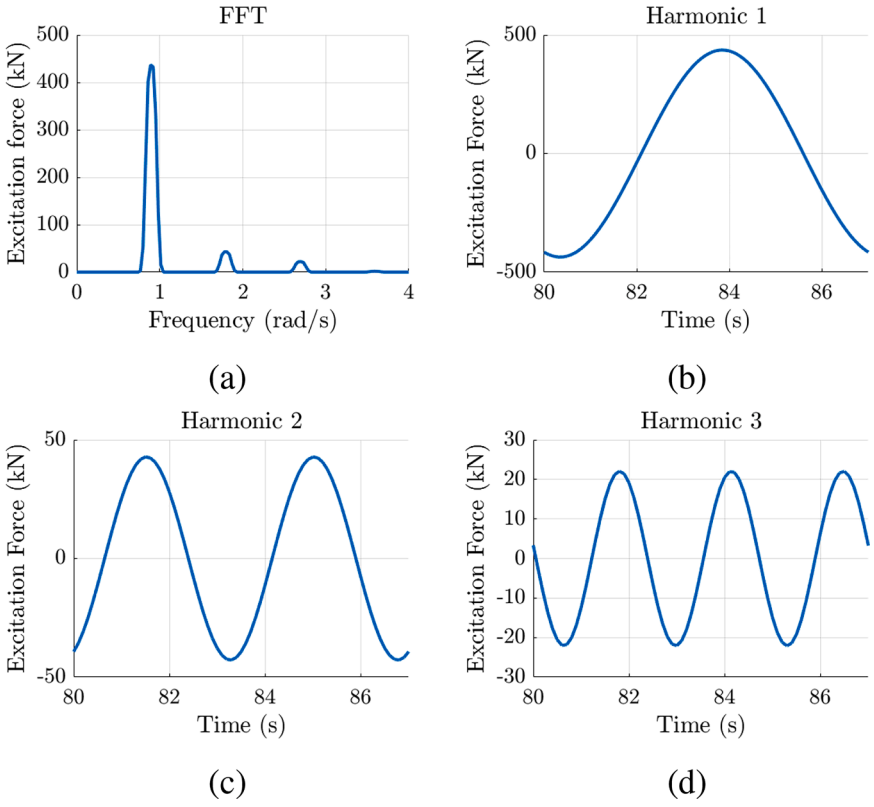

Fig. 5. (a) Frequency response of the nonlinear excitation signal shown in Fig. 4, and the decomposed signals of that in three harmonics shown in (b)–(d) separately.

implemented in MATLAB/Simulink (Giorgi , 2019). The computational convenience of NLFK4ALL is verified with WEC-Sim (Giorgi et al., 1971), and its accuracy is validated with the experimental wave tank data (Giorgi et al., 2020). On the other hand, the Kalman Filter is tuned for multi-resonant control to minimise the errors in signal decomposition of the nonlinear excitation force shown in Fig. 3.

The average excited power to the WEC system contained within the incoming waves, average power absorbed by the WEC, and the mean power losses caused by radiation and viscous drag forces are defined separately as follows:

$$\overline{P}_{exc} = \frac{1}{T}\int_0^T F_{exc}(t)\dot{z}(t)dt, \tag{25}$$

$$\overline{P}_{pto} = -\frac{1}{T}\int_0^T F_{pto}(t)\dot{z}(t)dt, \tag{26}$$

$$\overline{P}_{r} = \frac{1}{T}\int_0^T F_{r}(t)\dot{z}(t)dt, \tag{27}$$

$$\overline{P}_{vd} = \frac{1}{T}\int_0^T F_{vd}(t)\dot{z}(t)dt, \tag{28}$$

where T is the data collection period including a number of wave cycles after steady state; F_{exc}, F_{pto}, F_r, F_{vd} and $\dot{z}$ are the instantaneous total excitation force, PTO force, radiation force, viscous drag force and buoy velocity respectively. To remove the transient dynamic response, only the last 10 cycles (out of the total 40 simulated cycles) are used to calculate the average power output in the regular waves. Typical wave periods from 5 s to 10 s with an increment of 1 s are used in the simulations, so the corresponding wave frequencies range from 0.63 rad/s to 1.26 rad/s. The wave height is set to 2 m unless otherwise stated.

All results are implemented in regular waves. Although regular waves are less realistic compared to irregular waves, it is more deliberate to choose regular waves in this study to observe the impact of nonlinear hydrodynamics on the performance of controllers in both optimal and sub-optimal conditions. Nonlinearities generate higher harmonics at higher wave frequencies in the performance of a WEC system (e.g., the WEC displacement, and excitation force), which are clearly evident only with regular waves. Also, a clear discussion of the behaviour of the multi-resonant control (one of the main objectives of the paper) is more unequivocal with regular waves (albeit the authors acknowledge that quantifying its actual relevance requires realistic irregular waves, that is beyond the scope of this paper).

3. Results

The impact of predominant hydrodynamic nonlinearities (e.g., NLFK force, and viscous drag) on the linear control principles in regular waves will be demonstrated in Section 3.1. A comparison of optimal PI and multi-resonant controllers across different wave frequencies under nonlinear hydrodynamics will be shown in Section 3.2.

3.1. The impact of predominant hydrodynamic nonlinearities on the power of PI control following linear control principles

As mentioned in Section 2.4, predominant nonlinear hydrodynamics will be introduced into LM separately following Eqs. (9), (10), (11), and (13) to investigate the impact of each nonlinear term on the performance of linear control principles in regular waves. The power of each force component in each model is shown in Fig. 6 except for the hydrostatic term, which only plays a role in bringing the oscillating body to its equilibrium position and makes no contribution to the power of a WEC system. The blue bar denotes the power performance of a WEC system with linear PI control following linear control principles through Eqs. (19) and (20), while the orange bar denotes that with PI control achieving power maximisation in each model, where the optimal values of both parameters (K_{pto} and B_{pto}) are found by grid search mentioned

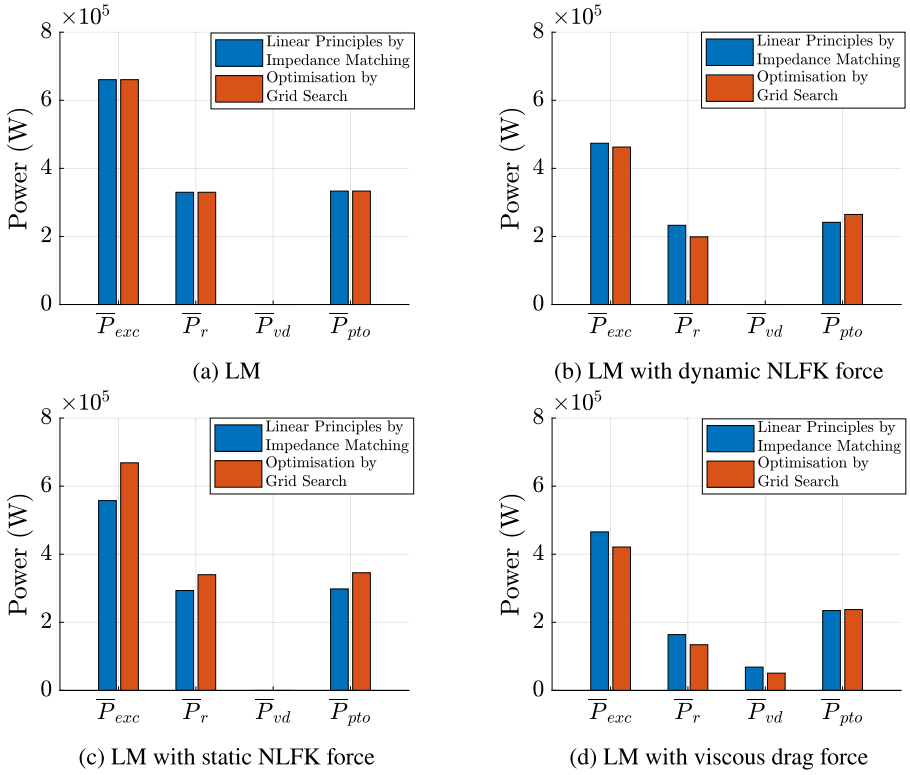

Fig. 6. Magnitudes of mean power for each component in Eq. (8) for a semi-submerged HPA when the controller follows linear control principles derived from impedance matching control (denoted as the blue bar) and with optimisation for power maximisation by grid search (denoted as the orange bar) based on (a) a linear-wave-theory model (LM), (b) LM with dynamic NLFK force, (c) LM with static NLFK force, and (d) LM with viscous drag force in regular waves with 2 m wave height and 0.89 rad/s wave frequency in regular waves.

in Section 2.5.2. Fig. 6a shows the results based on LM without any nonlinearities following Eq. (9). Fig. 6b and c show the results when the linear excitation and hydrostatic forces in LM are replaced by dynamic and static NLFK forces separately following Eqs. (10) and (11). Fig. 6d demonstrates the results with the introduction of viscous drag into LM following Eq. (13). The mean power calculations of excited power, absorbed power, radiated power, and viscous drag power follow Eqs. (25), (26), (27) and (28) respectively. The results shown in this section are based on regular wave conditions with a wave frequency of 0.89 rad/s (7 s wave period), and wave height of 2 m as an example.

3.1.1. *Excitation force (nonlinear dynamic Froude–Krylov force)*

In LM shown in Fig. 6a, when the incoming wave acts on the buoy, the mean power from linear excitation ($\overline{P}_{exc}$) contained in the waves inputs to the WEC system. Based on the linear optimal control principles following Eq. (21), half of the excited power is absorbed by the PTO controller, and another half is radiated back to the sea. Thus the power ratio between the absorbed ($\overline{P}_{pto}$) and excited power is maximum of 50 % following linear control principles. The optimal control gains can be obtained from optimal conditions analytically following Eqs. (19) and (20). Thus, the blue bar and orange bar show identical results in Fig. 6a.

As shown in Fig. 6b, the dynamic NLFK force is combined with a linear diffraction force as a nonlinear excitation force to replace the linear one in LM, while the other nonlinear forces (e.g., static NLFK, viscous drag) are not considered in this case. The introduction of dynamic NLFK force has a significant impact on the power in WEC systems, including both excited and absorbed power under optimal power maximising PTO control (denoted by the orange bar). At this sea state (2 m wave height, 0.89 rad/s wave frequency) under optimal PTO control, the excited power in the heave mode is reduced by 28 % under nonlinear excitation force, as compared with that under linear excitation force, shown in Fig. 6a. The same study is also conducted at 2 m wave height and wave frequencies ranging from 0.63 rad/s to 1.26 rad/s (10 s to 5 s wave periods) as shown in Fig. 16 in Appendix A. The reduction of wave excited power ranges from 17 % to 38 % with the decrease of the wave frequency (increase of nonlinear behaviour). Comparing the blue and orange bars in Fig. 6b, the results show that the linear control principles underestimate the absorbed power of WEC systems under medium to high sea states, which demonstrates the limitation of the linear control principle on the power performance of WEC systems under dynamic NLFK force. Even though the excited power is smaller under optimal control compared with that following linear control principles, the absorbed power is higher. On the other hand, the dynamic NLFK force has an implication on the power ratio between absorbed power and excited power. Under nonlinear excitation force, the maximum absorbed power is 59 % of the total available wave power when the optimal power maximising control is achieved, as compared with a maximum of 50 % under linear excitation force. The same study is also tested in a range of wave frequencies from 0.63 rad/s to 1.26 rad/s at the same wave height as shown in Fig. 17 in Appendix A. The power ratio between absorbed power and excited power also changes from 54 % to 68 % with the decrease of the wave frequency.

To further investigate the power ratio under a nonlinear excitation force, Fig. 7 plots the power versus buoy velocity in LM (denoted as a solid curve), and LM with dynamic NLFK force (denoted as a dashed curve) separately, where the red dot states the maximum absorbed power. The results in Fig. 7 are obtained when the optimal resonant condition is always achieved. The radiation power (the yellow curve) shows identical results across a range of velocities regardless of the existence of dynamic NLFK force because F_r is linear in this study, while the excited power has more nonlinear behaviour compared with that in the linear case. Therefore, the optimal velocity under dynamic NLFK force is 29 % lower than that in the linear case, and thus the absorbed

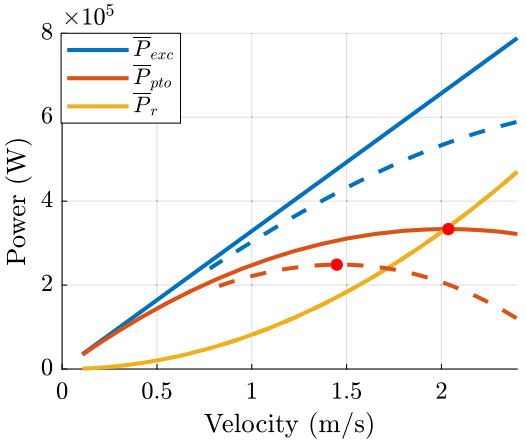

Fig. 7. Power of the WEC system versus buoy velocity with linear PI control under both linear (represented as a solid curve) and nonlinear (represented as a dashed curve) excitation forces when the optimal resonant condition is always achieved in regular waves with 2 m wave height and 0.89 rad/s wave frequency. The red dot denotes the maximum value of $\overline{P}_{pto}$ (orange curve).

power under dynamic NLFK force is much lower than that in the linear case.

To further investigate the limitations of linear control principles under nonlinear excitation force, Fig. 8a and b demonstrate the power versus various B_{pto} and K_{pto} separately to find out the optimal control gains under nonlinear excitation force. Fig. 8a shows the power in the WEC system versus different values of B_{pto} when the optimal K_{pto} is always achieved under both linear (solid curve) and nonlinear (dashed curve) excitation force. Note that the optimal control gains under linear excitation force can be obtained analytically from the linear optimal conditions following Eqs. (19) and (20), while that can only be obtained by a grid search under nonlinear excitation force. Fig. 8b shows the results of K_{pto} when the optimal B_{pto} is always achieved. The results in Fig. 8 show that linear wave theory underestimates the optimal damping and spring coefficient by 4 % and 8 % separately under nonlinear excitation force in regular waves with 2 m wave height and 0.89 rad/s wave frequency. The underestimations on PTO gains cause 9 % and 10 % power reductions separately compared with that under optimal control. The error of overestimation on control gains can be increased with the decrease of the wave frequency. Consequently, the linear control principles are not valid under the dynamic NLFK force, and both K_{pto} and B_{pto} have to be optimised.

3.1.2. Hydrostatic force (nonlinear static Froude–Krylov force)

Many previous studies stated that NLFK force is the most important hydrodynamic force affecting the buoy motion of HPAs (Giorgi and Ringwood, 2018; Davidson and Costello, 2020). Thus, the static NLFK force is introduced into the LM following Eq. (11). Comparing the power performance of WECs in Fig. 6a and c under static NLFK force with optimal power maximising control (represented as an orange bar), the results demonstrate that the power of each force component in the WEC system shows similar results to that under linear case. Fig. 9 further demonstrates that although the magnitude of static NLFK force takes a great proportion in the total hydrodynamic forces in a WEC system (denoted as a black bar), it has no effect on the power of the HPA WEC systems under optimal control, since the role of hydrostatic force is to bring the oscillating body to its equilibrium position (Falnes, 2002).

On the other hand, if PI control follows the linear control principle under static NLFK force, the maximum absorbed power of the WEC (represented as a blue bar) decreases compared with that under optimal control (represented as an orange bar) in Fig. 6c. Thus, the linear control principles may be violated by static NLFK force. Based on Eq. (19), the impact of static NLFK force is mainly on the linear optimal resonant condition. Therefore, the K_{pto} in the controller needs to be optimised to cancel out the influence of the static NLFK force, which can be obtained by the grid search method as mentioned in Section 3.1.1. Fig. 10a demonstrates that if the PI control follows the linear optimal resonant conditions stated in Eq. (19) under static NLFK force, the phase between the buoy velocity and excitation force is shifted by around 15 degrees at a steady state. Thus, the linear resonant condition fails to be achieved and the absorbed power of WEC decreases. Fig. 10b demonstrates that the phase shift is eliminated and the optimal resonant condition can be achieved after the optimisation by a grid search on K_{pto}.

Based on the linear control principles, the optimal amplitude condition should not be greatly influenced by the static NLFK force. To verify this hypothesis, Fig. 11 sets the controller following the linear control principle, achieving optimal amplitude condition only (denoted as Optimal B_{pto}), achieving optimal resonant condition only (denoted as Optimal K_{pto}), and achieving both optimal resonant and amplitude conditions under static NLFK force, separately. Fig. 11 demonstrates that compared with the PI control following linear control principle (denoted

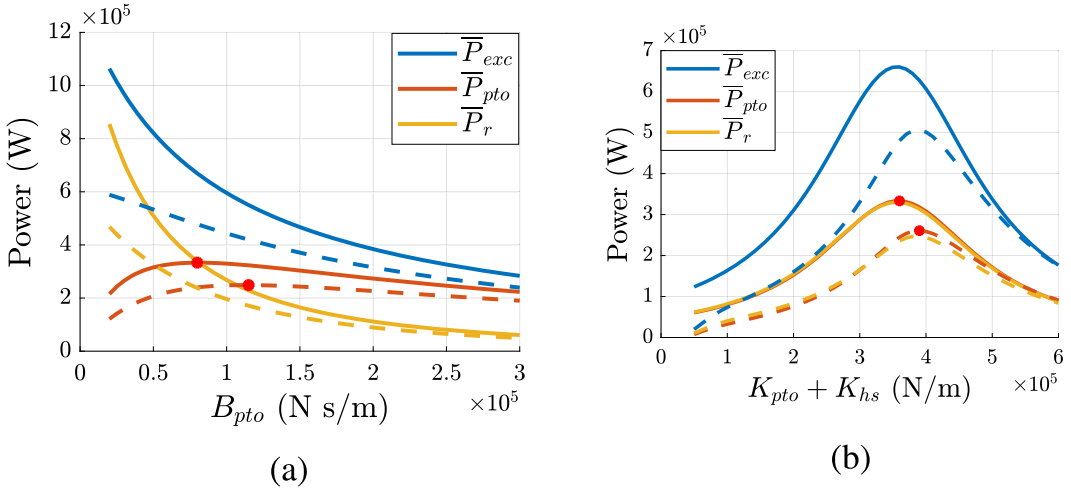

Fig. 8. Mean power arising from wave excitation and mean power output: radiated power and PTO absorbed power, versus variations in the (a) PTO damping coefficient while the optimal resonant condition is always achieved under both linear (solid curve) and nonlinear excitation forces (dashed curve), and (b) the PTO spring coefficient while the optimal amplitude condition is always achieved under both linear and nonlinear excitation forces. The red dot denotes the maximum value of $\overline{P}_{pto}$ (orange curve). The wave conditions are described by regular waves with 2 m height and a frequency of 0.89 rad/s.

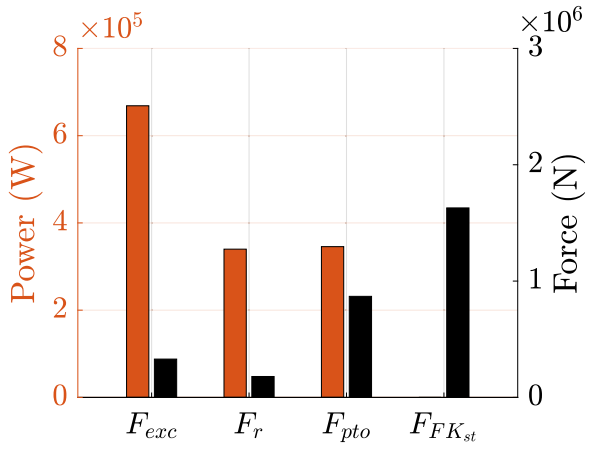

Fig. 9. Power and magnitude of force (rms value) for each force component in Eq. (8) for a semi-submerged HPA with optimal PI control under LM with static NLFK force in regular waves with 2 m wave height and 0.89 rad/s wave frequency.

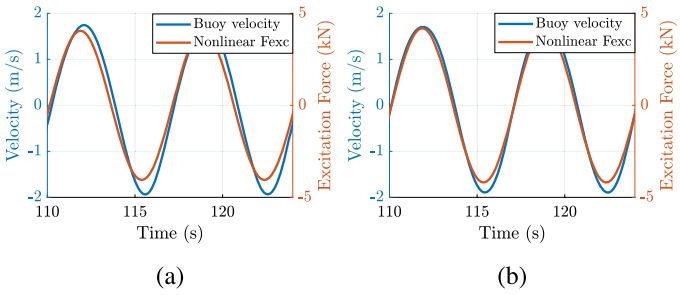

Fig. 10. Time series data of buoy velocity and nonlinear excitation force for a semi-submerged heaving PA with (a) linear PI control following linear optimal conditions, and (b) PI control achieving optimal resonant condition under static NLFK force in regular waves with 2 m wave height and 0.89 rad/s wave frequency.

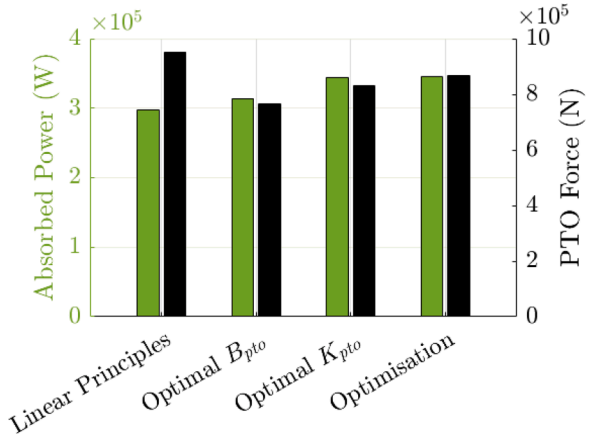

Fig. 11. Both the absorbed power and the PTO force (rms value) of WEC with linear PI control following linear optimal conditions (labelled as Linear Principles), PI control achieving optimal amplitude condition (labelled as Optimal B_{pto}), PI control achieving optimal resonant condition (labelled as Optimal K_{pto}), and PI control achieving optimisation on both resonant and amplitude conditions (labelled as Optimal Control) under static NLFK force in regular waves with 2 m wave height and 0.89 rad/s wave frequency.

as Linear Principles in Fig. 11), the PI achieving optimal resonant condition (denoted as Optimal K_{pto}) presents more absorbed power by 15 % in regular waves with 2 m wave height and 0.89 rad/s wave frequency. The same study is also demonstrated in a range of wave frequencies from 0.63 rad/s to 1.26 rad/s as shown in Fig. 18 in Appendix A, where the PI control with optimal resonant condition shows 1 % to 54 % more power than that following linear control principles with the decrease of wave frequency. By contrast, the results with PI achieving optimal amplitude condition only (denoted as Optimal B_{pto}) are very close to that with the PI control following linear control principle. Therefore, the static NLFK force has a minor impact on the optimal value of B_{pto}. On the other hand, the PTO control force decreases compared with that under linear principles. The reason for that is there is less $F_{FK_{st}}$ as stated in Fig. 11, so less K_{pto} is required to achieve optimal resonant condition. Thus, in Eq. (22), the required control force to achieve optimisation is less, which is also observed in some of the literature (Mérigaud and Ringwood, 2017). Consequently, the static NLFK force can cause phase shift between the buoy velocity and the excitation force, and thus the linear optimal resonant condition is not valid under the static NLFK force.

3.1.3. Viscous drag

Viscous drag, as one of the most common hydrodynamic nonlinearities, is also considered in this paper. The viscous drag force was stated as showing less relevance in HPAs than the other hydrodynamic forces (e.g., NLFK force, and radiation force) since the magnitude of that is smaller than other forces(Giorgi and Ringwood, 2018). However, viscous drag has a non-negligible effect on the linear optimal amplitude conditions of the PTO control in Eq. (20), and thus the power of WEC systems. The viscous drag term accounts for 30 % of the total dissipative terms (radiated power and viscous drag power) in Fig. 6d in regular waves with 2 m wave height and 0.89 rad/s wave frequency. Also, the power performance of an HPA WEC is significantly reduced by viscous drag. The absorbed power is reduced by 29 % under viscous drag with optimal control (represented as an orange bar) compared with that in LM, shown in Fig. 6a. The same test is implemented across different wave frequencies from 0.63 rad/s to 1.26 rad/s as shown in Fig. 19 in Appendix A. The absorbed power is reduced by 17 %-57 % with the decrease of wave frequency.

To investigate the impact of viscous drag on the optimal gains, Fig. 12 demonstrates that the absorbed power of a WEC system with PI control following linear control principles shows similar results (by 3 %) to that with optimal power maximising control (denoted as Optimal Control). The same analysis is implemented across different wave frequencies from 0.63 rad/s to 1.26 rad/s as shown in Fig. 20 in Appendix A. The absorbed power is improved by 1–6 % with the decrease of wave frequency. Therefore, the results show that the Lorentz-linearised B_{vd}^{ω} in the linear control principle can have a good estimation for achieving the maximum power absorption under viscous drag, so the linear control principle is valid under viscous drag. Nevertheless, the power ratio of the absorbed power over excited power is 56 % under optimal control as shown in Fig. 12, as compared with 50 % estimated by Lorentz Linearisation in linear control principles.

It is demonstrated that some nonlinear hydrodynamics (e.g., the dynamic and static NLFK forces) may make the linear PTO control principles invalid in real-time implementation. Meanwhile, the dynamic NLFK and viscous drag forces have a significant impact on the power performance of an HPA WEC under optimal control. Thus, the partially nonlinear model assembling dynamic and static NLFK forces and viscous drag following Eq. (14) is implemented in this paper for further study as shown in Fig. 13. Comparing with Fig. 6, the power of each component in Eq. (8) is further decreased under the combination of nonlinear hydrodynamics aforementioned. In addition, the linear control principle is not valid in this partially nonlinear model.

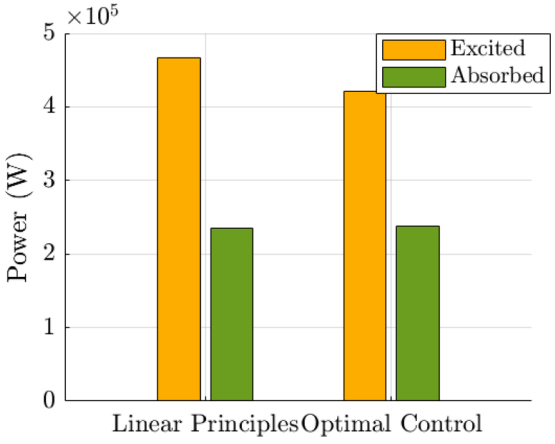

Fig. 12. Both mean excited power and absorbed power of WEC with linear PI control following linear optimal conditions (labelled as Linear Principles), and PI control achieving optimisation on both resonant and amplitude conditions (labelled as Optimal Control) under viscous drag force in regular waves with 2 m wave height and 0.89 rad/s wave frequency.

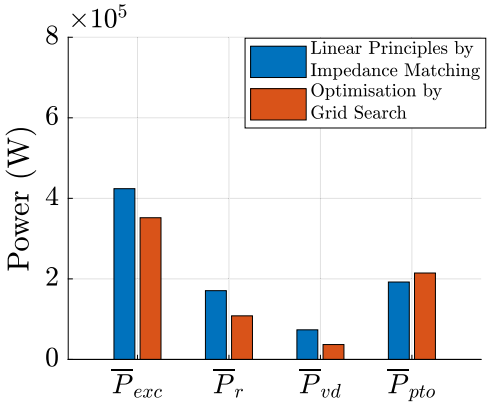

Fig. 13. Magnitudes of mean power for each component in Eq. (8) for a semi-submerged HPA following linear control principles derived from impedance matching control (denoted as the blue bar) and with optimisation by grid search (denoted as the orange bar) based on a partially nonlinear model with dynamic and static NLFK forces, and viscous drag force in regular waves with 2 m wave height and 0.89 rad/s wave frequency in regular waves.

3.2. The comparison of PI and multi-resonant controls under nonlinear hydrodynamics

As mentioned in Section 2.5.3, the measurement data may contain multiple harmonics signals with different amplitudes and phases under nonlinearities, which may cause some complex control problems (e.g., tuning). Thus, multi-resonant control is introduced into the WEC system to improve the power performance under nonlinearities. In this section, the partially model with both static and dynamic NLFK forces and viscous drag force is implemented. A comparison of PI and multi-resonant control on the power performance is presented in Fig. 14 in regular waves with 2 m wave height and 0.89 rad/s wave frequency.

There are 5 scenarios tested, where S1 is based on LM without any nonlinearities following Eq. (9), while S2 to S5 are based on both dynamic and static NLFK forces with viscous drag following Eq. (14):

- S1: Optimal PI control following the linear control principle.
- S2: Non-optimal PI control following the linear control principle.
- S3: Non-optimal multi-resonant control following the linear control principle.
- S4: Optimal PI control through a grid search.
- S5: Optimal multi-resonant control through a grid search.

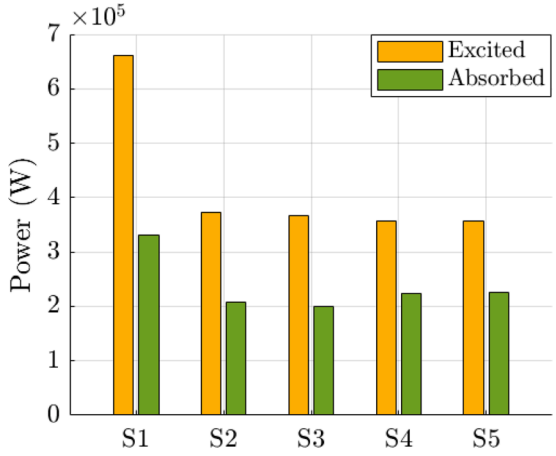

Fig. 14. Mean power from wave excitation and mean PTO absorbed power in 5 scenarios with PI and multi-resonant controllers for a semi-submerged heaving PA in regular waves with 2 m wave height and 0.89 rad/s wave frequency.

If both controllers follow linear control principles under nonlinearities, the multi-resonant control (S3) shows similar results to PI (S2) control on both excited (2 % lower than PI) and absorbed power (3 % lower than PI). After the optimisation through a grid search, multi-resonant control (S5) shows almost identical power to PI (S4). The same investigation is implemented in a range of wave frequencies from 0.63 rad/s to 1.26 rad/s with 2 m wave height. The absorbed power of a multi-resonant control shows 1 % to 4 % more than that of PI with the decrease of wave frequencies. It is surprising to observe that there is no outstanding power performance from multi-resonant control in regular waves, since it is designed to parallelly optimise the PTO performance based on different harmonics in the incoming wave, and its outstanding power performance was demonstrated in irregular waves (Song et al., 2016).

Further analysis is shown in Fig. 15, which demonstrates the excited power at fundamental frequency (Fig. 15a) and at the second and third harmonics (Fig. 15) across wave frequencies.

Although the nonlinear excitation force exhibits harmonics at second and third wave frequencies as shown in Fig. 5, the available wave power in the second and third wave frequencies is 2–3 magnitudes lower than the available wave power in the fundamental wave frequency. Therefore, although the multi-resonant control is designed to optimise the power in each harmonic, the maximum absorbed power in the second and third harmonics can be neglected compared with that in the fundamental one. Consequently, the results demonstrate that compared with multi-resonant control, traditional linear PI control is able to achieve the optimal power absorption after optimisation under both dynamic and static NLFK forces and viscous drag in regular waves.

4. Discussion

The results presented in this paper aim to solve two research questions, as mentioned in Section 1. The conclusions are based on a spherical HPA since predominant nonlinear hydrodynamics (e.g., NLFK force) have more significant impact on that than other types of WECs, as mentioned in Section 2.1.

4.1. What is the limitation of linear control principles on the power performance of an PA exhibiting nonlinear dynamics?

Controller can achieve optimisation for power absorption following linear wave theory in LM. However, the introductions of both dynamic and static NLFK forces violate linear control principles in medium to high sea states. When the dynamic NLFK force is included in the WEC system, neither linear resonant nor amplitude conditions are valid, so the controllers need to be re-tuned under dynamic NLFK force. When

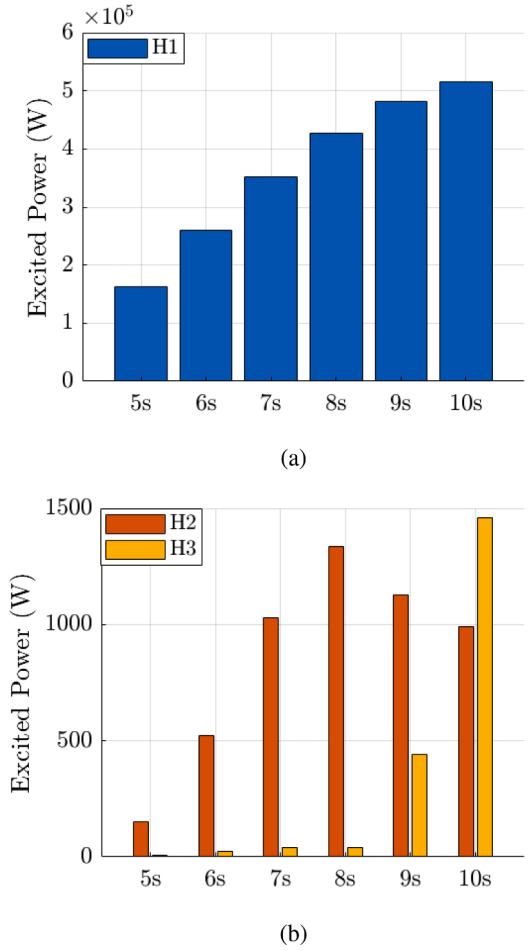

Fig. 15. Mean power from the excitation force at the (a) fundamental frequency and (b) second and third harmonics with 2 m wave height across wave periods from 5 s to 10 s (0.63 rad/s to 1.26 rad/s wave frequencies) for a semi-submerged heaving PA.

the static NLFK force is considered, it causes a phase shift between excitation and buoy velocity, and thus has a significant impact on the linear resonant condition, while the linear amplitude condition is valid. Consequently, linear control principles are only valid under NLFK force in small sea states, which comprises 2 m wave height and 5 s wave period in regular waves. Once the wave height increases, the tunings of controllers that closely follow linear control principles (e.g., ACC, and AVT) are greatly impacted by nonlinear NLFK forces. The linear control principles underestimate the absorbed power by up to 54 % across wave frequencies from 0.63 rad/s to 1.26 rad/s under NLFK forces, as compared with the actual optimal control.

On the other hand, it is expected that under hydrodynamic nonlinearities, the power will be influenced under optimal power maximisation control in medium to high sea states, as compared with that in a linear model. However, the previous literature stated that the viscous drag has a minor impact on the PA WECs (Giorgi and Ringwood, 2018), while the results in this paper demonstrate that the viscous drag forces cause significant reduction on both excited power (up to 51 %) and absorbed power (up to 57 %) compared with that in linear cases across wave frequencies from 0.63 rad/s to 1.26 rad/s. Also, the dynamic NLFK force has implications for the power of an HPA, while the static NLFK force has a minor impact on that.

In this study, only a spherical HPA is considered. Although the NLFK forces has its greatest impact on the specific geometry of a buoy and on heave mode over other types of WECs, mode coupling is not considered, which may have an impact on the performance of controllers. On the other hand, a CFD solver/experiment is ideal for inclusion to further demonstrate the limitation of linear power maximising control principles in a more close-to real environment.

4.2. Is it possible or necessary to improve the linear control principles to maximise the absorbed power under predominant nonlinear dynamics?

In a partially nonlinear model with dynamic and static NLFK forces and viscous drag, the optimal PI control is able to achieve the optimal power absorption compared with the multi-resonant control. However, the linear optimal conditions are proved invalid under NLFK force. Thus, a specific tuning method of PI control is proposed to estimate the optimal control coefficients for power absorption to save optimisation time. The simulations are tested for a semi-submerged spherical HPA across typical regular waves (5 s to 10 s wave periods, and 1 m to 2 m wave heights). Eqs. (29) and (30) state the estimations of optimal stiffness and damping coefficients under dynamic and static NLFK and viscous drag forces based on linear optimal conditions in Eqs. (19) and (20).

$$K_{pto} = \omega^2(m + a \cdot A^{\omega}) - k_{hs}, \tag{29}$$

$$B_{pto} = b \cdot T_w B_r^{\omega} + c \cdot T_w H_w B_{vd}^{\omega}, \tag{30}$$

where a, b and c are 0.14, 0.17 and 0.4 respectively. Since radiation damping and added mass coefficients are wave-frequency dependent, the estimation on their optimal values needs to take the wave period (frequency) into consideration. Similarly, the linearised viscous damping is both wave frequency and wave amplitude dependent as mentioned in Section 3.1.3, so both are considered in the estimation. Eqs. (29) and (30) are valid in regular waves with wave heights ranging from 1m to 2 m, and with wave periods ranging from 5 s to 10 s (0.63 rad/s to 1.26 rad/s wave frequencies). The error between the maximum absorbed powers obtained from estimated and optimised control gains are within 8 %.

The multi-resonant control is a wind band control that shows similar power performance as CCC control in irregular waves (Song et al., 2016). However, the previous studies only consider the implementation of multi-resonant control in linear models to decompose the signal in a wave spectrum into multiple wave frequencies (Abdelkhalik et al., 2017). In this study, multi-resonant control is able to decompose the complex signals from hydrodynamic nonlinearities with sub controllers, and optimise the control gains at each harmonic. However, multi-resonant control does not show outstanding power performance over traditional PI control under predominant nonlinear hydrodynamics in regular waves in this study. The main reason is the excited power in the fundamental wave frequencies is in the order of two to three magnitude higher than that in other harmonics. Thus, the control effects from other harmonics play a minor role on the performance of WEC systems. However, there are more nonlinear hydrodynamics in reality, which can generate more super-harmonics. Thus, multi-resonant control has more potential benefits than traditional PI control to solve nonlinear signals in the further studies.

5. Conclusion

In this paper, predominant hydrodynamic nonlinearities are chosen to assemble a partially nonlinear model. The focus of this paper is to answer the research questions listed in Section 1 regarding the ongoing controversies between nonlinear hydrodynamics (reality) and linear PTO control (feasibility in implementation). The results demonstrate the limit of linear control principles under both dynamic and static NLFK forces under medium to high sea states. On the other hand, the power performance of multi-resonant control is stated and compared with that of PI control under predominant nonlinear hydrodynamics. An estimated tuning method derived from linear control principles is proposed to estimate the optimal control gains across typical regular waves for a semi-submerged spherical HPA, which saves much computational time to achieve the optimisation of controllers.

Future work will focus on improving the power performance of controllers (e.g., multi-resonant controller) under predominant nonlinear hydrodynamics in irregular waves, which more accurately represent real sea states. Also, motion constraints will be included in the WEC models, which is lacking in this paper.

CRediT authorship contribution statement

Yifeng Gu: Writing – review & editing, Writing – original draft, Visualization, Validation, Supervision, Software, Resources, Project administration, Methodology, Investigation, Formal analysis, Data curation, Conceptualization; **Boyin Ding:** Writing – review & editing, Supervision, Project administration, Methodology, Investigation, Formal analysis, Conceptualization; **Nataliia Y. Sergiienko:** Writing – review & editing, Supervision, Software, Methodology, Investigation, Formal analysis, Conceptualization; **Benjamin S. Cazzolato:** Writing – review & editing, Supervision, Methodology, Investigation, Formal analysis;
Giuseppe Giorgi: Writing – review & editing, Software, Resources, Formal analysis

Declaration of competing interest

The authors declare that they have no known competing financial interests or personal relationships that could have appeared to influence the work reported in this paper.

Appendix A. Results in more sea states

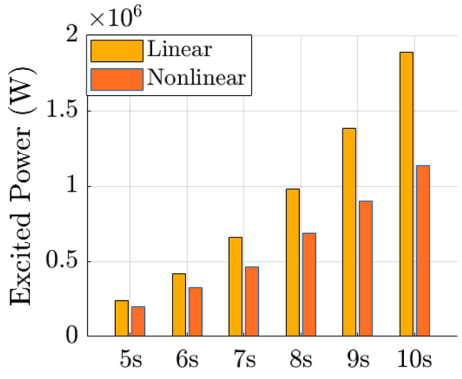

Fig. 16. Mean excited power from incoming waves with optimal PI control in LM (labelled as Linear) and LM with dynamic NLFK force models (labelled as Nonlinear) for a semi-submerged heaving PA in the regular waves with 2 m wave height and different wave periods.

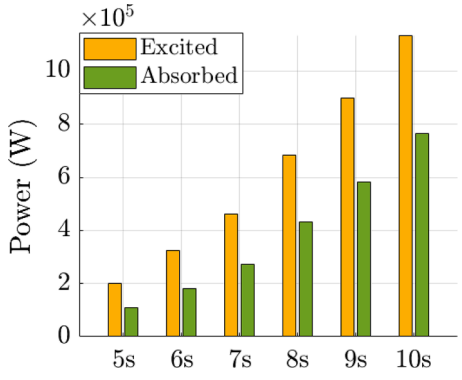

Fig. 17. Mean excited power from incoming waves and mean PTO absorbed power with optimal PI control under dynamic NLFK force for a semi-submerged heaving PA in the regular waves with 2 m wave height and different wave periods.

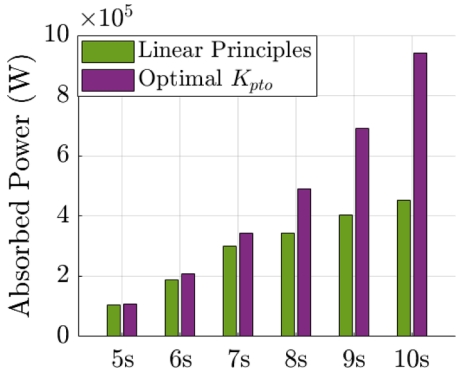

Fig. 18. Mean absorbed power of WEC with linear PI control following linear optimal conditions (labelled as Linear Principles), PI control achieving optimal resonant condition (labelled as Optimal K_{pto}) under static NLFK force for a semi-submerged heaving PA in the regular waves with 2 m wave height and different wave periods.

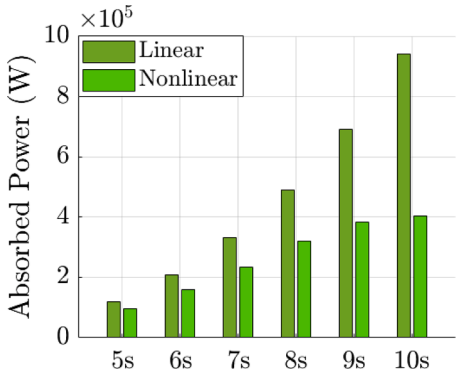

Fig. 19. Mean absorbed power of WEC with optimal PI control in LM (labelled as Linear) and LM with viscous drag models (labelled as Nonlinear) for a semi-submerged heaving PA in the regular waves with 2 m wave height and different wave periods.

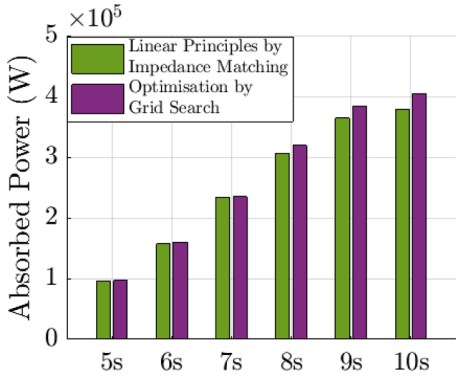

Fig. 20. Mean absorbed power of WEC with linear PI control when the controller follows linear optimal conditions derived from impedance matching control (labelled as Linear Principles by Impedance Matching), and that with optimisation for power maximisation by grid search (labelled as Optimisation by Grid Search) under viscous drag for a semi-submerged heaving PA in the regular waves with 2 m wave height and different wave periods.

References

Abdelkhalik, O., Zou, S., 2019. Control of small two-body heaving wave energy converters for ocean measurement applications. Renew. Energy 132, 587–595.
Abdelkhalik, O., Zou, S., Robinett, R.D., Bacelli, G., Wilson, D.G., Coe, R., Korde, U., 2017. Multiresonant feedback control of a three-degree-of-freedom wave energy converter. IEEE Trans. Sustain. Energy 8 (4), 1518–1527.
Agency, I. R.E., 2014. Ocean Energy: Technologies, Patents, Deployment Status and Outlook. International Renewable Energy Agency.

Al Shami, E., Wang, Z., Wang, X., 2021. Non-linear dynamic simulations of two-body wave energy converters via identification of viscous drag coefficients of different shapes of the submerged body based on numerical wave tank CFD simulation. Renew. Energy 179, 983–997.

Babarit, A., Delhommeau, G., 2015. Theoretical and numerical aspects of the open source BEM solver NEMOH. In: 11th European Wave and Tidal Energy Conference (EWTEC2015).

Babarit, A.l., Mouslim, H., Cleément, A., Laporte-Weywada, P., 2009. On the numerical modelling of the non linear behaviour of a wave energy converter. In: International Conference on Offshore Mechanics and Arctic Engineering. Vol. 43444, pp. 1045–1053.

Bacelli, G., Coe, R.G., 2020. Comments on control of wave energy converters. IEEE Trans. Control Syst. Technol. 29 (1), 478–481.

Coe, R.G., Bacelli, G., Wilson, D.G., Abdelkhalik, O., Korde, U.A., Robinett III, R.D., 2017. A comparison of control strategies for wave energy converters. Int. J. Mar. Energy 20, 45–63.

Davidson, J., Costello, R., 2020. Efficient nonlinear hydrodynamic models for wave energy converter design—A scoping study. J. Mar. Sci. Eng. 8 (1), 35.

Do, D.K., 2022. Nonlinear control with wave observer to maximize harvested power for point absorber wave energy converters. Asian J. Control 24 (1), 16–45.

Faedo, N., Carapellese, F., Pasta, E., Mattiazzo, G., 2022a. On the principle of impedance-matching for underactuated wave energy harvesting systems. Appl. Ocean Res. 118, 102958.

Faedo, N., Giorgi, G., Ringwood, J.V., Mattiazzo, G., 2022b. Optimal control of wave energy systems considering nonlinear froude–krylov effects: control-oriented modelling and moment-based control. Nonlinear Dyn. 109 (3), 1777–1804.

Falnes, J., 1995. On non-causal impulse response functions related to propagating water waves. Appl. Ocean Res. 17 (6), 379–389.

Falnes, J., 2002. Ocean Waves and Oscillating Systems: Linear Interactions Including Wave-Energy Extraction. Cambridge University Press.

Falnes, J., Perlin, M., 2003. Ocean waves and oscillating systems: linear interactions including wave-energy extraction. Appl. Mech. Rev. 56 (1), B3.

Folley, M., 2016. Numerical Modelling of Wave Energy Converters: State-of-the-Art Techniques for Single Devices and Arrays. Academic Press.

Gilloteaux, J.-C., Bacelli, G., Ringwood, J., 2008. A non-linear potential model to predict large-amplitudes-motions: application to a multi-body wave energy converter. WREC.

Giorgi, G., 2024. The onset of instability in a parametric resonance energy harvester under panchromatic excitations. Int. J. Mech. Sci. 281, 109544.

Giorgi, G., Gomes, R.P.F., Henriques, J.C.C., Gato, L.M.C., Bracco, G., Mattiazzo, G., 2020. Detecting parametric resonance in a floating oscillating water column device for wave energy conversion: numerical simulations and validation with physical model tests. Appl. Energy 276, 115421.

Giorgi, G., 2019. Nonlinear Froude–Krylov Matlab demonstration toolbox. https://doi.org/10.5281/zenodo.3517130.

Giorgi, G., Penalba, M., Gomes, R. P.F., 1971. Code-to-code nonlinear hydrodynamic modelling verification for wave energy converters: WEC-sim vs. NLFK4ALL. Proceedings of the European Wave and Tidal Energy Con Ference, 1971–1.

Giorgi, G., Ringwood, J., 2017a. Consistency of viscous drag identification tests for wave energy applications. In: Proceedings of the 12th European Wave and Tidal Energy Conference 27th Aug–1st Sept 2017. European Wave and Tidal Energy Conference 2017, pp. 1–8.

Giorgi, G., Ringwood, J.V., 2017b. Nonlinear Froude–Krylov and viscous drag representations for wave energy converters in the computation/fidelity continuum. Ocean Eng. 141, 164–175.

Giorgi, G., Ringwood, J.V., 2018. Comparing nonlinear hydrodynamic forces in heaving point absorbers and oscillating wave surge converters. J. Ocean Eng. Mar. Energy 4, 25–35.

Gobato, R., Gobato, A., Fedrigo, D., 2016. Harnessing the energy of ocean surface waves by pelamis system. Energy 2 (2), 1–15.

Gu, Y., Ding, B., Sergiienko, N.Y., Cazzolato, B.S., 2021. Power maximising control of a heaving point absorber wave energy converter. IET Renew. Power Gener. 15 (14), 3296–3308.

Guo, B., Ringwood, J.V., 2021. A review of wave energy technology from a research and commercial perspective. IET Renew. Power Gener. 15 (14), 3065–3090.

Kara, F., 2020. A control strategy to improve the efficiency of point absorber wave energy converters in complex sea environments. J. Mar. Sci. Res. Oceanogr. 3 (2), 46–54.

Kim, S.-J., Koo, W., Kim, M.-H., 2021. The effects of geometrical buoy shape with nonlinear Froude–Krylov force on a heaving buoy point absorber. Int. J. Nav. Archit. Ocean Eng. 13, 86–101.

MARINTEK, T., Norway, J., 2002. The specialist committee on waves .

Merigaud, A., Gilloteaux, J.-C., Ringwood, J.V., 2012. A nonlinear extension for linear boundary element methods in wave energy device modelling. In: International Conference on Offshore Mechanics and Arctic Engineering. Vol. 44915. American Society of Mechanical Engineers, pp. 615–621.

Mérigaud, A., Ringwood, J.V., 2017. Optimal trajectories, nonlinear models and constraints in wave energy device control. IFAC-PapersOnLine 50 (1), 15645–15650.

Morison, J.R., Johnson, J.W., Schaaf, S.A., 1950. The force exerted by surface waves on piles. J. Pet. Technol. 2 (05), 149–154.

Newman, J.N., 2018. Marine Hydrodynamics. The MIT Press.

Penalba, M., Giorgi, G., Ringwood, J.V., 2017. Mathematical modelling of wave energy converters: a review of nonlinear approaches. Renew. Sustain. Energy Rev. 78, 1188–1207.

Penalba Retes, M., Mérigaud, A., Gilloteaux, J.-C., Ringwood, J., 2015. Nonlinear Froude–Krylov force modelling for two heaving wave energy point absorbers. In: Proceedings of the 11th European Wave and Tidal Energy Conference. European Wave and Tidal Energy Conference 2015.

Perez, T., Fossen, T.I., 2009. A matlab toolbox for parametric identification of radiation-force models of ships and offshore structures. Model., Identif. Control 30 (1), 1–15.

Richter, M., Magana, M.E., Sawodny, O., Brekken, T. K.A., 2012. Nonlinear model predictive control of a point absorber wave energy converter. IEEE Trans. Sustain. Energy 4 (1), 118–126.

Ringwood, J.V., Bacelli, G., Fusco, F., 2014. Energy-maximizing control of wave-energy converters: the development of control system technology to optimize their operation. Control Syst., IEEE 34 (5), 30–55.

Sergiienko, N., Cazzolato, B., Hardy, P., Arjomandi, M., Ding, B., 2017. Internal-model-based velocity tracking control of a submerged three-tether wave energy converter. In: Proceedings of the Twelfth European Wave and Tidal Energy Conference, Cork, Ireland.

Sergiienko, N.Y., 2018. Three-tether wave energy converter: hydrodynamic modelling, performance assessment and control. Ph.D. thesis. Univ. Adelaide.

Song, J., Abdelkhalik, O., Robinett, R., Bacelli, G., Wilson, D., Korde, U., 2016. Multi-resonant feedback control of heave wave energy converters. Ocean Eng. 127, 269–278.

Tedd, J., Frigaard, P., 2007. Short term wave forecasting, using digital filters, for improved control of wave energy converters. In: The Seventeenth International Offshore and Polar Engineering Conference. OnePetro.

Terra, G.M., van de Berg, W.J., Maas, L. R.M., 2005. Experimental verification of Lorentz' linearization procedure for quadratic friction. Fluid Dyn. Res. 36 (3), 175.